The Astrophysical Journal, 810:148 (17pp), 2015 September 10 doi:10.1088/0004-637X/810/2/148

FIVE GROUPS OF RED GIANTS WITH DISTINCT CHEMICAL COMPOSITION IN THE GLOBULAR CLUSTER NGC 2808*

Eugenio Carretta
INAF, Osservatorio Astronomico di Bologna, via Ranzani 1, I-40127, Bologna, Italy; eugenio.carretta@oabo.inaf.it
Received 2015 July 2; accepted 2015 July 24; published 2015 September 8

ABSTRACT

The chemical composition of multiple populations in the massive globular cluster (GC) NGC 2808 is addressed with the homogeneous abundance reanalysis of 140 red giant branch stars. UVES spectra for 31 stars and GIRAFFE spectra for the other giants were analyzed with the same procedures used for about 2500 giants in 23 GCs in our FLAMES survey, deriving abundances of Fe, O, Na, Mg, Si, Ca, Ti, Sc, Cr, Mn, and Ni. Iron, elements from α capture, and those in the Fe group do not show intrinsic scatter. On our UVES scale, the metallicity of NGC 2808 is [Fe/H] $= -1.129 \pm 0.005 \pm 0.034$ ($\pm$ statistical $\pm$ systematic error) with $\sigma = 0.030$ (31 stars). The main features related to proton-capture elements are retrieved, but the improved statistics and the smaller associated internal errors allow us to uncover five distinct groups of stars along the Na–O anticorrelation. We observe large depletions in Mg, anticorrelated with enhancements of Na and also Si, suggestive of unusually high temperatures for proton captures. About 14% of our sample is formed by giants with solar or subsolar [Mg/Fe] ratios. Using the [Na/Mg] ratios, we confirm the presence of five populations with different chemical compositions that we call *P1*, *P2*, *I1*, *I2*, and *E* in order of decreasing Mg and increasing Na abundances. Statistical tests show that the mean ratios in any pair of groups cannot be extracted from the same parent distribution. The overlap with the five populations recently detected from UV photometry is good but not perfect, confirming that more distinct components probably exist in this complex GC.

Key words: stars: abundances – stars: atmospheres – stars: Population II

Supporting material: machine-readable tables

1. INTRODUCTION

Galactic globular clusters (GCs) host multiple stellar populations of widely (sometimes wildly) different chemical composition and slightly different ages, as shown for a long time by spectroscopy and more recently by photometric studies (see the review by Gratton et al. 2012 for a summary of observations, references, and topics on GCs).

The first evidence from abundance analyses in the last two decades of the past century revealed clear C–N and Na–O anticorrelations, as well as the first correlations between Na and Al abundances in a few GCs, reviewed by, for example, Smith (1987) and Kraft (1994). Very different abundances of these light elements in coeval stars at the same evolutionary stage in otherwise monometallic stellar aggregates did negate the very same definition of a simple stellar population. However, this concept was not abandoned until two milestones were reached. First, theory provided the understanding that the observed abundance patterns could be generated by the simultaneous action of the NaNa and MgAl cycles in the same stratification where the ON part of the CNO cycle is operating in H burning at high temperature (e.g., Denisenkov & Denisenkova 1989; Langer et al. 1993). Second, the first observation of the Na–O and Mg–Al anticorrelations among unevolved GC stars (Gratton et al. 2001) unambigously demonstrated that the Na, Al-enhanced and O,Mg-depleted composition must be inherited by the most massive stars of a (or several) previous stellar generation(s).

Since then, the (anti)correlations among proton-capture elements have been understood to represent the true DNA of GCs. These relations distinguish cluster stars from the other phylum of Pop. II field stars, where only the basic evolutionary effects—first dredge-up and a second mixing episode after the red giant branch (RGB) bump in the luminosity function—on the lightest C and N elements are observed (Gratton et al. 2000). The best-studied chemical signature is the Na–O anticorrelation, discovered by the Lick-Texas group (see Kraft 1994; Sneden 2000) and so widespread that it can be considered as the fingerprint of a bona fide GC (Carretta et al. 2010b). The ubiquity of this important tracer shows that almost all GCs are composed of multiple populations.

The more recent photometric approach to multiple populations in GCs exploits the presence in the filter passbands of absorption features of proton-capture elements. In most cases, only the lightest elements C or N are involved, with impact on those blue/near-UV filters, including NH, CN, and CH features (e.g., Grundahl et al. 1998; Marino et al. 2008; Han et al. 2009; Lee et al. 2009; Milone et al. 2012a; Monelli et al. 2013, and references therein). Using pseudocolor indexes, where stars of different generations are more or less separated owing to the different chemical compositions, it is at present routinely possible to uncover broad or split photometric sequences in most GCs. The recent addition of the F275W passband of the Wide-Field Camera 3 (WFC3 camera) (Piotto et al. 2015), which samples an OH molecular band, is useful to connect these photometric sequences with heavier proton-capture elements like O (and Na, through the NeNa and ON cycles). Although no photometric filter seems to be presently able to detect differences in the heaviest elements involved in proton-capture reactions (Mg, Al, Si), space-based UV photometry confirms that most GCs are formed by multiple populations.

However, some GCs are more multiple than others. The most recent case is NGC 2808, where Milone et al. (2015)

* Based on data collected at the ESO telescopes under program 072.D-0507 and during the FLAMES Science Verification program.

separated five distinct populations using a combination of F275W, F336W, and F438W filters from the *Hubble Space Telescope* (*HST*). NGC 2808 is a pivotal object to investigate in detail the complex scenario of the origin of multiple populations in GCs, exploiting the wealth of photometric and spectroscopic data gathered for this cluster. Apart from ω Cen and M54, whose metallicity spread tells a tale of a different origin (probably in or as a core of a former dwarf nucleated galaxy), NGC 2808 is the fifth most massive object in the catalog by Harris (1996) of Galactic GCs ($M_V = -9.39$). The present-day total mass is found to be the driving parameter in establishing the extent of chemical differences among multiple populations (Carretta et al. 2010b). Moreover, the cluster mass is one of the more relevant factors (together with the metallicity) in determining whether proton-capture reactions are able to proceed to temperatures high enough to significantly affect the primordial level of heavier elements like Mg, from SNe II (Carretta et al. 2009b).

Three distinct main sequences (MSs) have long been known to exist in this GC (Piotto et al. 2007; Milone et al. 2012b), one of the best examples of the impact on the color–magnitude diagrams (CMDs) of helium, the main outcome of the H burning at high temperature. The distribution of stars along its horizontal branch (HB) is multimodal (Bedin et al. 2000) and reaches quite a hot effective temperature, again a good signature of enhanced He abundance in a fraction of stars.

Our group has been actively working for many years on the chemical composition of stars in NGC 2808, gathering an unprecedented wealth of data. The first evidence of multiple populations in this cluster came from the analysis of Na abundances in 81 giants from moderately high resolution FLAMES spectra (Carretta et al. 2003). The spread in [Na/Fe][1] was found to span a range of about 1 dex, similar to what was found in other GCs by the Lick-Texas group. Soon after, Carretta et al. (2004) confirmed the multiple populations in NGC 2808 by finding an extended Na–O anticorrelation on the RGB from high-resolution UVES spectra of 20 stars, with [O/Fe] ratios as low as -1 dex. This is not surprising because there is a tight correlation between the extent of the Na–O anticorrelation and the maximum temperature along the HB (Carretta et al. 2007d), both features driven again by the same factor, He. NGC 2808 was one of the GCs used by Carretta (2006) to define the interquartile range of the [O/Na] ratio, IQR[O/Na], as an efficient way to quantify the extension of the Na–O anticorrelation and the relevance at large of changes in chemical composition due to the process of formation of a GC and its multiple populations. An abundance analysis of HB stars was presented by Gratton et al. (2011) and Marino et al. (2014).

The analysis of GIRAFFE spectra for 120 giants in NGC 2808 (Carretta et al. 2006) started our FLAMES survey devoted to studying the link between Na–O anticorrelation and HB in about 25 GCs (Carretta et al. 2006, 2007a, 2007b, 2007c, 2009b, 2009c, 2010c, 2011, 2013a, 2014, 2015; Gratton et al. 2006, 2007). However, being the first target considered in the survey, NGC 2808 was analyzed with slightly different procedures from those used for the other GCs, in particular the scale of effective temperatures, efficiently tuned for all other GCs to minimize the impact of uncertainties in the atmospheric parameters on star-to-star errors in abundances. This inconsistency calls for a reanalysis of all the available material to derive the chemical composition of stars in NGC 2808 in a homogeneous way with respect to the other GCs in the survey.

The first results of this reanalysis concerning the Al abundances (only available for 31 RGB stars with UVES spectra) were already presented in Carretta (2014) along with Mg abundances. The stars were found clustered into three discrete groups with different chemical compositions along the Mg–Al anticorrelation. The fractions of stars in the three components were found to be in excellent agreement with the number ratios computed by Milone et al. (2012b) on the three MSs.

In the present paper we provide the full derivation of the atmospheric parameters for all stars with available spectra from previous analyses. For 31 giants with UVES data, we derived abundances of Fe, O, Na, Si, Ca, Ti, Sc, Cr, Mn, and Ni. Homogeneous abundances of Fe, O, and Na are derived again for the 123 giants with GIRAFFE spectra, and new abundances of Mg, Si, Ca, Ti, Sc, Cr, and Ni were obtained for the first time for this large set of stars. Homogeneous abundance ratios in our total sample extend the analysis of discrete components along the RGB of NGC 2808.

The paper is organized as follows. In Section 2 we describe the analysis method and the derivation of the atmospheric parameters with associated errors, and the results for abundances. The Na–O and Na–Mg anticorrelations are presented in Section 3, and the chemical tagging of multiple populations in NGC 2808 is discussed in Section 4. Finally, in Section 5 we summarize our findings.

2. ANALYSIS

2.1. Sample

The observational material of the present reanalysis consists of UVES spectra for 31 red giants and GIRAFFE spectra for 123 giants, all acquired with the FLAMES instrument (Pasquini et al. 2002) at the ESO VLT-UT2 telescope. We used proprietary UVES data (ESO Program 072.D-0507) for 12 stars analyzed in Carretta et al. (2009b) and UVES spectra from the FLAMES Science Verification for 19 stars whose analysis was done in Carretta et al. (2004) and Carretta (2006). These spectra have a resolution of $R \sim 47{,}000$ and a spectral range between 4800 and 6800 Å, with a small gap at about 5900 Å. Coordinates and magnitudes for all 31 stars of the UVES sample can be found in Carretta (2014).

The GIRAFFE spectra were taken with the high-resolution grating and two setups, HR11 ($R = 24{,}100$, wavelength range 5597–5840 Å) and HR13 ($R = 21{,}900$, wavelength range 6120–6405 Å). In this GIRAFFE sample, 32 stars were observed with HR11 only, 28 with HR13 only, and 63 have observations with both setups. Coordinates and magnitudes for these giants are in Carretta et al. (2006). Details of the observations and data reduction are reported in the original papers.

Fourteen out of 154 RGB stars were observed with both UVES and GIRAFFE, so our final sample consists of 140 individual stars, all members of the RGB of NGC 2808 (see the original papers by Carretta et al. 2004, 2006), spanning the magnitude range $V = 13.34 \div 16.44$. In Figure 1 the location of these RGB stars on the V, $B - V$ CMD from Bedin et al. (2000) is shown. Only one star is fainter than the RGB-bump

[1] We adopt the usual spectroscopic notation, i.e., $[X] = \log(X)_{\rm star} - \log(X)_{\odot}$ for any abundance quantity X, and $\log \epsilon(X) = \log (N_X/N_{\rm H}) + 12.0$ for absolute number density abundances.

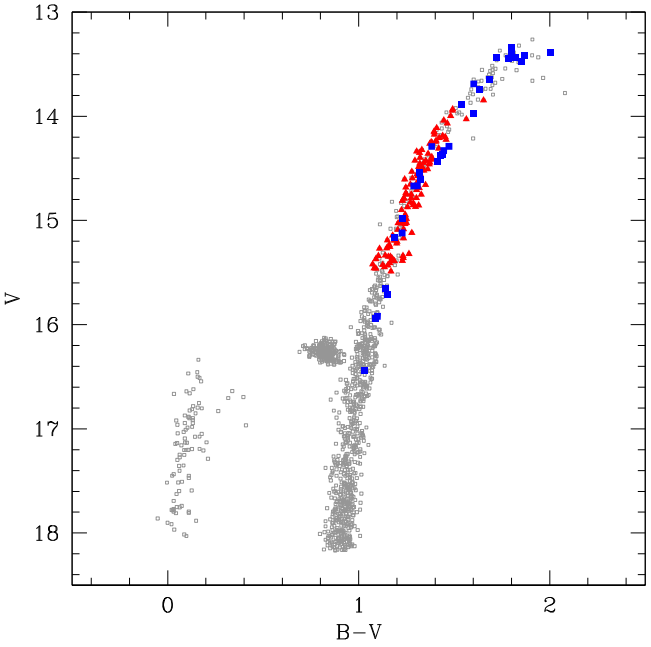

Figure 1. V, $B-V$ CMD of NGC 2808 (Bedin et al. 2000, small squares). Stars in the present sample observed with UVES are indicated with large blue squares, and giants observed with GIRAFFE are represented by large red triangles.

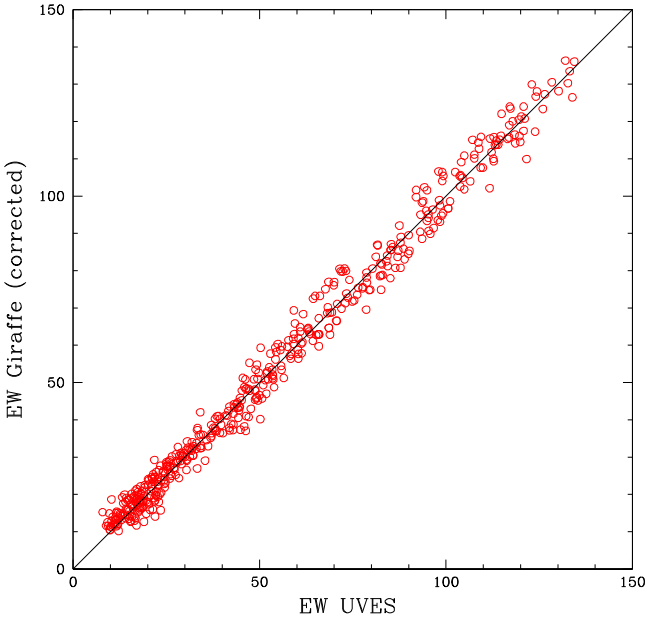

Figure 2. EWs measured on GIRAFFE spectra, after the correction to the UVES systems, as a function of the EWs measured on UVES spectra for the 14 giants observed with both spectrographs.

level $V = 16.235$ (Nataf et al. 2011). The optical photometry was integrated with K-band magnitudes from the Point Source Catalog of Two Micron All-Sky Survey (2MASS) (Skrutskie et al. 2006) to derive atmospheric parameters, as described in the next section.

2.2. Atmospheric Parameters and Metallicity

All the abundances derived in the present reanalysis rest on equivalent widths (EWs) measured with the procedure described in Bragaglia et al. (2001) and using the latest version of the package ROSA (Gratton 1988). A first difference with the original analysis in Carretta et al. (2006) is that this time the EWs measured on the GIRAFFE spectra were corrected to the system defined by EWs from the higher resolution UVES spectra. We used a linear regression between the two sets of measurements derived using 478 lines in common for the 14 stars observed with both instruments. The corrected EWs from GIRAFFE are plotted as a function of the UVES EWs in Figure 2.

This is the first step to make the present analysis perfectly consistent with the abundance analysis of more than 2500 RGB stars in the other GCs observed in our FLAMES survey.

The second step concerns the effective temperature ($T_{\rm eff}$) scale. In Carretta et al. (2004, 2006) and Carretta (2006), the giants of our sample were analyzed using $T_{\rm eff}$ values derived from $V-K$ colors and the calibration by Alonso et al. (1999, 2001). The new approach followed for the other 23 GCs and adopted here also for NGC 2808 is to use the above temperatures as first-pass values: the final values adopted for all our target stars were obtained using an average relation between $T_{\rm eff}\,(V-K)$ and the K apparent magnitudes of the RGB stars. This adopted procedure has three advantages: it decreases the star-to-star scatter in abundances due to uncertainties in temperatures (magnitudes are more precise than colors), it minimizes the impact of the differential reddening in NGC 2808 on derived $T_{\rm eff}$, and finally it is fully consistent with the procedure adopted for all other GCs.

Surface gravities $\log g$ were obtained from bolometric corrections (from Alonso et al.), the newly derived effective temperatures, reddening, and distance modulus from Harris (1996), and assuming masses of 0.85 $M_{\odot}$ and $M_{\rm bol,\odot} = 4.75$ as the bolometric magnitude for the Sun.

Finally, values of the microturbulent velocity v_t were obtained by eliminating in each star trends of the abundances from Fe I lines with the expected line strength (see Magain 1984). Final abundances were derived from an EW analysis, by choosing the model in the Kurucz (1993) grid of solar-scaled LTE model atmospheres with the overshooting option switched on, with the proper atmospheric parameters, whose abundance matched the one derived from Fe I lines. The adopted line list, atomic parameters, and solar reference abundances are described in Gratton et al. (2003).

The new, final atmospheric parameters are listed with the derived Fe abundances of the 140 individual stars in Table 1.

NGC 2808 is confirmed to be monometallic, as far as the content of iron is concerned. On the homogeneous metallicity scale based on high-resolution UVES spectra (Carretta et al. 2009a), the metal abundance in NGC 2808 is on average [Fe/H] I $= -1.129 \pm 0.005 \pm 0.034$ dex ($\sigma = 0.030$) from the 31 stars observed with UVES (where the first and second error bars refer to the statistical and systematic errors, respectively; see next section). From the reanalysis of the 123 stars with GIRAFFE spectra, we derive on average [Fe/H] I $= -1.128 \pm 0.002 \pm 0.046$ dex ($\sigma = 0.026$). We then are entitled to merge the two subsamples, adopting the values from UVES for all abundances in the 14 stars observed with both instruments. The improvement due to the new homogeneous procedure is immediately evident in the decrease of the rms scatters associated with the mean Fe values, the previous values being $\sigma = 0.075$ and $\sigma = 0.065$ for UVES and GIRAFFE, respectively.

Table 1
Adopted Atmospheric Parameters and Derived Iron Abundances in NGC 2808

Star	$T_{\rm eff}$ (K)	log g (dex)	[A/H] (dex)	v_t (km s^{-1})	n	[Fe/H] I (dex)	rms	n	[Fe/H] II (dex)	rms
7183	4531	1.52	−1.08	1.70	46	−1.080	0.071	4	−1.121	0.257
7315	4459	1.45	−1.14	1.29	54	−1.138	0.086	3	−1.075	0.078
U7536	4306	1.18	−1.11	1.55	89	−1.109	0.079	10	−1.125	0.055
7558	4711	1.87	−1.13	1.64	47	−1.129	0.086	4	−1.106	0.270
7788	4510	1.53	−1.15	1.44	20	−1.144	0.058	...	...	...

Note. The prefix U indicates stars observed with UVES.

(This table is available in its entirety in machine-readable form.)

Abundances of iron derived from singly ionized transitions are in very good agreement with the above values. We derived [Fe/H] II $= -1.128$ dex ($\sigma = 0.026$ dex, 31 stars) and [Fe/H] II $= -1.143$ dex ($\sigma = 0.033$ dex, 91 stars) from the UVES and GIRAFFE samples, respectively.

Derived abundances of [Fe/H] I and [Fe/H] II are plotted as a function of the effective temperatures in Figure 3, together with internal, star-to-star error bars as estimated in the next subsection.

2.3. Abundances and Error Analysis

Abundances of Fe, O, Na, Mg, Al, Si, Ca, Ti, Cr, Mn, and Ni for 19 giants with UVES spectra from the FLAMES Science Verification were originally presented in Carretta et al. (2004) and Carretta (2006). O, Na, Mg, Al, and Si for the 12 RGB stars observed with UVES in our FLAMES survey were analyzed originally with the other 202 stars in 17 GCs in Carretta et al. (2009b). These abundances are derived again using the new scale of atmospheric parameters discussed above for all 31 stars of the UVES sample and are presented here for the first time, except for abundances of Al and Mg (Carretta 2014). For these stars, the abundances of Ti and Cr were obtained using both neutral and singly ionized species, with the results in excellent agreement.

For the 123 stars in the GIRAFFE sample, Fe, O, and Na were revisited with respect to the values in Carretta et al. (2006), obtained with the previous temperature scale and without correcting the EWs to the UVES system. Abundances of Mg, Si, Ca, Ti, Cr, and Ni are obtained for the first time in the present analysis. Due to the limited spectral range of GIRAFFE spectra, only transitions of neutral Ti and Cr were available for this set of giants.

Abundances of Na were corrected for the effects of departures from the LTE assumption using prescriptions by Gratton et al. (1999), whereas abundance corrections for Sc and Mn as in Gratton et al. (2003) were adopted to account for the hyperfine structure.

In summary, we obtained homogeneous abundances of the elements O, Na, Mg, and Si involved in proton-capture reactions. Moreover, we derived the abundances of elements representative of the α-capture process (Ca, Ti) and of the Fe group (Sc, Cr, Mn, Ni). Average abundance ratios and their rms scatter are listed in Table 2, where the average value of Al by Carretta (2014) is also indicated. The abundances are listed separately for the UVES and GIRAFFE sets, but whenever possible we adopted UVES abundances for individual stars in our merged sample.

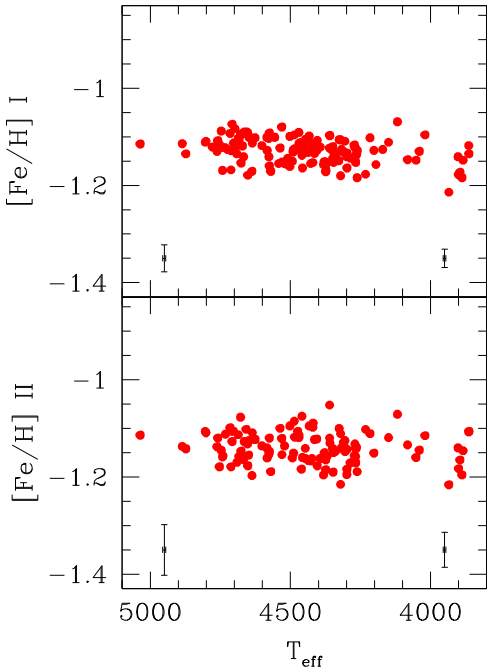

Figure 3. Abundance ratios [Fe/H] I (upper panel) and [Fe/H] II (lower panel) as a function of $T_{\rm eff}$ for all 140 RGB stars in the present reanalysis. Error bars on the right and on the left side are star-to-star errors for targets observed with UVES and GIRAFFE, respectively.

Table 2
Mean Abundances from UVES and GIRAFFE

Element	UVES n avg rms	GIRAFFE n avg rms
[O/Fe] I	31 +0.06 0.34	91 +0.00 0.38
[Na/Fe] I	31 +0.20 0.20	123 +0.24 0.23
[Mg/Fe] I	31 +0.26 0.16	122 +0.27 0.16
[Al/Fe] I	31 +0.46 0.47	...
[Si/Fe] I	31 +0.29 0.07	123 +0.30 0.05
[Ca/Fe] I	31 +0.33 0.02	123 +0.33 0.03
[Sc/Fe] II	31 −0.01 0.04	123−0.00 0.05
[Ti/Fe] I	31 +0.21 0.02	123 +0.22 0.04
[Ti/Fe] II	29 +0.18 0.02	...
[Cr/Fe] I	31 −0.04 0.02	123−0.03 0.03
[Cr/Fe] II	31 −0.03 0.03	...
[Mn/Fe] I	31 −0.37 0.04	...
[Fe/H] I	31 −1.13 0.03	123−1.13 0.03
[Fe/H] II	31 −1.14 0.03	91 −1.14 0.03
[Ni/Fe] I	31 −0.06 0.02	123−0.08 0.02

Note. Individual abundances of Al are reported in Carretta (2014).

Table 3
Sensitivities of Abundance Ratios to Variations in the Atmospheric Parameters and to Errors in the Equivalent Widths, and Errors in Abundances for Stars of NGC 2808 Observed with UVES and GIRAFFE

Element	Average *n.* Lines	$T_{\rm eff}$ (K)	log *g* (dex)	[A/H] (dex)	v_t (km s^{-1})	EWs (dex)	Total Internal	Total Systematic
UVES								
Variation		50	0.20	0.10	0.10			
Internal		5	0.04	0.03	0.05	0.01		
Systematic		46	0.06	0.03	0.01			
[Fe/H] I	71	+0.036	+0.015	+0.003	−0.031	0.009	0.019	0.034
[Fe/H] II	9	−0.055	+0.102	+0.031	−0.015	0.027	0.036	0.059
[O/Fe] I	2	−0.022	+0.067	+0.029	+0.028	0.057	0.061	0.066
[Na/Fe] I	4	+0.011	−0.048	−0.034	+0.013	0.040	0.043	0.040
[Mg/Fe] I	3	−0.009	−0.013	−0.006	+0.016	0.046	0.047	0.029
[Al/Fe] I	2	+0.007	−0.023	−0.011	+0.021	0.057	0.058	0.086
[Si/Fe] I	7	−0.050	+0.020	+0.008	+0.021	0.030	0.033	0.048
[Ca/Fe] I	15	+0.027	−0.031	−0.015	−0.017	0.021	0.024	0.027
[Sc/Fe] II	8	+0.048	−0.023	−0.004	−0.016	0.028	0.030	0.045
[Ti/Fe] I	9	+0.051	−0.019	−0.016	−0.005	0.027	0.028	0.047
[Ti/Fe] II	9	+0.041	−0.030	−0.010	−0.024	0.027	0.030	0.039
[Cr/Fe] I	17	+0.036	−0.030	−0.015	−0.007	0.019	0.021	0.035
[Cr/Fe] II	10	+0.016	−0.026	−0.017	+0.004	0.025	0.026	0.018
[Mn/Fe] I	3	+0.016	−0.012	−0.007	−0.015	0.046	0.047	0.016
[Ni/Fe] I	26	−0.011	+0.015	+0.006	+0.010	0.016	0.017	0.012
GIRAFFE								
Element	Average *n.* Lines	$T_{\rm eff}$ (K)	log *g* (dex)	[A/H] (dex)	v_t (km s^{-1})	EWs (dex)	Total Internal	Total Systematic
Variation		50	0.20	0.10	0.10			
Internal		5	0.04	0.03	0.08	0.01		
Systematic		46	0.06	0.05	0.01			
[Fe/H]I	37	+0.050	+0.005	−0.003	−0.030	0.013	0.028	0.046
[Fe/H]II	3	−0.039	+0.096	+0.027	−0.013	0.047	0.052	0.046
[O/Fe]I	2	−0.041	+0.079	+0.035	+0.035	0.057	0.067	0.060
[Na/Fe]I	3	−0.004	−0.037	−0.019	+0.016	0.047	0.049	0.024
[Mg/Fe]I	2	−0.014	−0.009	−0.004	+0.016	0.057	0.058	0.020
[Si/Fe]I	8	−0.051	+0.026	+0.012	+0.026	0.029	0.036	0.048
[Ca/Fe]I	5	+0.015	−0.029	−0.010	−0.019	0.036	0.040	0.016
[Sc/Fe]II	5	−0.055	+0.077	+0.031	+0.001	0.036	0.041	0.030
[Ti/Fe]I	4	+0.032	−0.013	−0.012	+0.006	0.041	0.041	0.056
[Cr/Fe]I	5	+0.014	−0.014	−0.007	+0.022	0.036	0.040	0.014
[Ni/Fe]I	8	−0.014	+0.017	+0.008	+0.021	0.029	0.033	0.014

The sensitivity of the derived abundances to variations in the adopted atmospheric parameters for each element was obtained by reiterating the analysis and varying each time only one parameter of the amount shown in Table 3. For the final slopes of the relations between the variation in each parameter and the abundance, we took the average over all stars. This computation was done separately for UVES and GIRAFFE.

These sensitivities were used to estimate the impact of uncertainties in atmospheric parameters on the derived abundances. A detailed description is given in Carretta et al. (2007a, 2009b), respectively, for the analysis of GIRAFFE and UVES spectra. We note here that with respect to the analysis of NGC 2808 in Carretta et al. (2006, 2009b), the internal error in temperature is now reduced by almost an order of magnitude, from 44 to 5 K, with the presently adopted procedure for $T_{\rm eff}$. This improvement is very important to minimize the star-to-star errors in abundances (Table 3), a crucial step for a meaningful study of a possible segregation of stars into groups with discrete chemical compositions.

3. RESULTS

For individual stars, abundances of proton-capture elements are given in Table 4. In Table 5 are listed abundances of α- and Fe-group elements for species measured both on UVES and GIRAFFE spectra. Abundances of Ti II, Cr II, and Mn (only available from UVES spectra) are listed in Table 6. The run of abundance ratios in NGC 2808 does not show any trend as a function of effective temperature.

We provide in Figure 4 a graphical summary of the derived abundances in NGC 2808, using the so-called box-and-whiskers plot (Tukey 1977), which is particularly well suited to visualizing possible skewed distributions and to investigating the presence of outstanding outliers.

Table 4
Abundances of Proton-capture Elements in Stars of NGC 2808

Star	n	[O/Fe]	rms	n	[Na/Fe]	rms	n	[Mg/Fe]	rms	n	[Si/Fe]	rms	limO
7183	2	+0.232	0.033	4	+0.135	0.023	3	+0.323	0.077	10	+0.261	0.084	1
7315	2	+0.352	0.047	4	−0.150	0.040	3	+0.363	0.101	12	+0.278	0.085	1
U7536	2	+0.248	0.040	4	+0.060	0.017	3	+0.355	0.095	8	+0.260	0.039	1
7558	1	+0.392	⋯	3	−0.076	0.067	2	+0.370	0.009	11	+0.249	0.072	1
7788	0	⋯	⋯	2	+0.224	0.026	1	+0.352	⋯	8	+0.236	0.066	1

Note. Upper limits (limO = 0) and detections (= 1) for O are flagged.

(This table is available in its entirety in machine-readable form.)

Table 5
Abundances of α- and Fe-peak Elements in Stars of NGC 2808

Star	n	[Ca/Fe]	rms	n	[Ti/Fe] I	rms	n	[Sc/Fe] II	rms	n	[Cr/Fe] I	rms	n	[Ni/Fe]	rms
7183	6	+0.326	0.059	5	+0.228	0.071	6	−0.066	0.071	5	−0.052	0.078	11	−0.077	0.087
7315	7	+0.317	0.113	5	+0.159	0.078	6	+0.039	0.151	3	−0.053	0.138	7	−0.123	0.031
U7536	13	+0.318	0.069	10	+0.189	0.047	8	−0.045	0.103	18	−0.051	0.089	30	−0.066	0.064
7558	7	+0.332	0.102	6	+0.215	0.072	6	−0.057	0.072	5	−0.061	0.081	10	−0.061	0.219
7788	1	+0.339	⋯	2	+0.236	0.042	5	+0.050	0.062	5	−0.024	0.121	2	−0.064	0.007

(This table is available in its entirety in machine-readable form.)

Table 6
Abundances of Ti II, Cr II, and Mn in Stars of NGC 2808 Observed with UVES

Star	n	[Ti/Fe] II	rms	n	[Cr/Fe] II	rms	n	[Mn/Fe]	rms
8739	9	+0.208	0.094	14	−0.011	0.118	3	−0.395	0.026
38660	8	+0.186	0.110	17	−0.048	0.174	3	−0.355	0.009
8603	9	+0.195	0.091	14	−0.071	0.120	3	−0.378	0.080
10571	8	+0.197	0.072	12	−0.020	0.067	3	−0.399	0.048
30763	9	+0.200	0.070	14	−0.034	0.133	3	−0.359	0.066

(This table is available in its entirety in machine-readable form.)

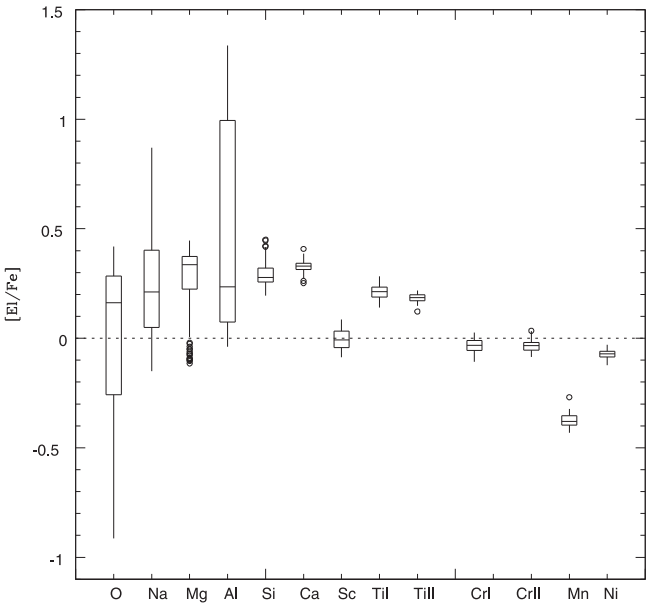

Figure 4. Box-and-whiskers plot of abundance ratios in RGB stars of NGC 2808. The horizontal line in each box is the median ratio of a given element. The bottom and top lines of the box are the 25th and 75th percentiles, respectively, whose distance (i.e., the box length) indicates the interquartile range, encompassing the middle 50% of the data. The vertical "whiskers" protruding from the box indicate the full abundance range excluding the outliers, defined as points lying more than 1.5 times the interquartile range from the 25th or 75th percentiles and indicated with open circles.

The abundance pattern observed in NGC 2808 is typical of massive, normal GCs. Light elements involved in proton-capture reactions present a huge spread, exceeding many times the uncertainties associated with the analysis. Pure α-process elements like Ca and Ti (not touched by proton-capture reactions, like instead Mg and Si) show a much more limited range, with overabundances typical of normal nucleosynthesis from SNe II. Similarly, species belonging to the Fe peak follow rather well the run of iron, apart from Mn, which is underabundant, as in normal halo stars of similar metallicity.

However, from this compact representation it is immediately clear that the Mg in NGC 2808 is outstanding even among proton-capture elements. The improved statistics of the present analysis, 140 RGB stars compared to the maximum of 31 stars with Mg abundance analyzed in Carretta (2014), allows us to uncover an unusually large number of outliers in the Mg distribution, all of them with subsolar [Mg/Fe] ratios. Also, the Si distribution seems to be peculiar, with a number of outliers located at the high-abundance border of the distribution, that is, anticorrelated with the behavior observed in Mg.

3.1. The Classic Na–O Anticorrelation

The updated version of the Na–O anticorrelation, the most outstanding typical signature of the chemical composition in a GC, is shown in Figure 5. Abundances of Na are available for all 140 stars in our merged sample because Na lines fall in both the HR11 and HR13 setups (and obviously in the UVES

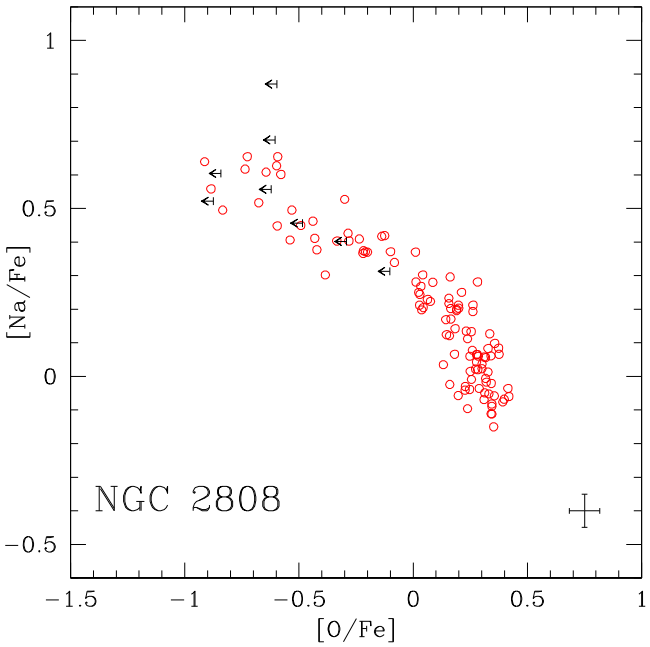

Figure 5. Anticorrelation of O and Na abundances in RGB stars of NGC 2808 from the present reanalysis. Arrows indicate upper limits in [O/Fe]. Star-to-star errors are those referred to the bulk of stars, observed with GIRAFFE. Internal errors for the 31 stars with UVES spectra are slighly smaller.

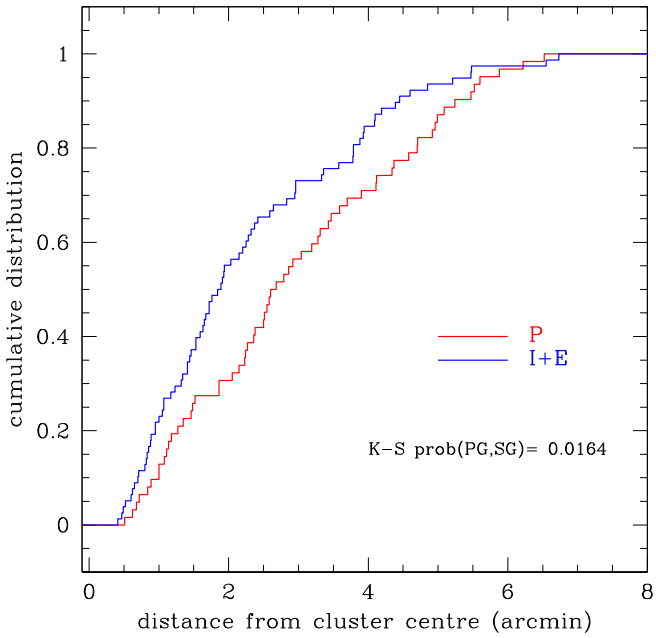

Figure 6. Cumulative distribution of radial distances from the cluster center for stars of first (*P* component) and of second (*I*+*E*) generation in NGC 2808. The probability of a Kolmogorov–Smirnov test is also listed.

spectral range). However, abundances of O are only available for 91 stars observed with the GIRAFFE setup HR13; when merged with the UVES sample, our final sample includes 117 stars with both O and Na, which is, however, the largest to date used to study this feature in a normal, monometallic GC.

The present reanalysis confirms many previous results (Carretta et al. 2006). The Na–O anticorrelation is very extended, showing stars with O abundances reaching almost [O/Fe] = −1 dex. The interquartile range of the [O/Na] ratio, IQR[O/Na], introduced by Carretta (2006) to provide a quantitative measure of changes in chemical composition between stars of different generations, is 0.925. This value, although slightly smaller than the old value (0.999), perfectly fits the relation with the cluster total present-day mass (as represented by the proxy of the total absolute magnitude M_V). In the same way, we confirm that NGC 2808 lies very well in the relation discovered by Carretta et al. (2007d), linking the extension of the Na–O anticorrelation with the HB morphology, as represented by the maximum temperature along the HB (Recio-Blanco et al. 2006).

The division of stars into the three components defined in Carretta et al. (2009c), primordial *P* and two components of second-generation stars with intermediate *I* and extreme *E* composition, gives the fractions $P = 46\% \pm 6\%$, $I = 36\% \pm 6\%$, and $E = 18\% \pm 4\%$, where the attached errors are from Poisson statistics. We confirm that NGC 2808 is one of the GCs where the highest fraction of first-generation stars was retained: almost half of the present-day stellar population belongs to the *P* component, whereas the observed mean over more than 20 GCs homogeneously analyzed by our group is that only a third of stars show a pristine composition.

Second-generation stars (components *I* and *E*) show a tendency to be more concentrated than stars with primordial composition (Figure 6): a two-tail Kolmogorov–Smirnov test allows us to safely reject the null hypothesis that the two distributions are extracted from the same parent population. However, due to the limitations imposed by the fiber positioning of FLAMES, only a small fraction of stars in our sample is located within two half-mass radii from the cluster center. Coupled to the different concentrations of first- and second-generation stars, this suggests that more ample photometric data sets are better suited for a more thorough study of this issue.

At first blush, there seems to not be much difference with respect to previous results. However, the improved statistics of the merged sample and the decrease of internal errors due to the atmospheric parameters uncover a more subtle level of complexity in this cluster. The distribution function of the [O/Na] ratio reveals that stars along the Na–O anticorrelation seem to be split not simply in three, but into several structures, namely five groups peaked at about [O/Na] = +0.30, 0.0, −0.65, −0.9, and −1.3 dex (see Figure 7).

Let us assume, as a working hypothesis, that both the *P* and *I* components in NGC 2808 are each composed of two subgroups. The separation of the last three peaks at low [O/Na] values in Figure 7 is quite large, but even considering conservatively the larger errors estimated for GIRAFFE, the distance between the first two peaks also exceeds by almost four times the combined internal uncertainty in O and Na (see Table 3). This means that the ensemble of stars with primordial composition in NGC 2808 is not a monolitic group, but rather composed by two subcomponents, with small differences in the average [O/Fe] ratio and larger differences in the Na content.

The existence of these two groups is in excellent agreement with the independent result obtained from the abundance analysis of HB stars in NGC 2808 by Gratton et al. (2011). By observing several tens of stars, they found some evidence of Na–O anticorrelation already among the red HB (RHB) stars that should be the descendents of He-poor, O-rich stars. Gratton et al. (2011) concluded that the stellar populations in NGC 2808 must be more than three because at least some of the red

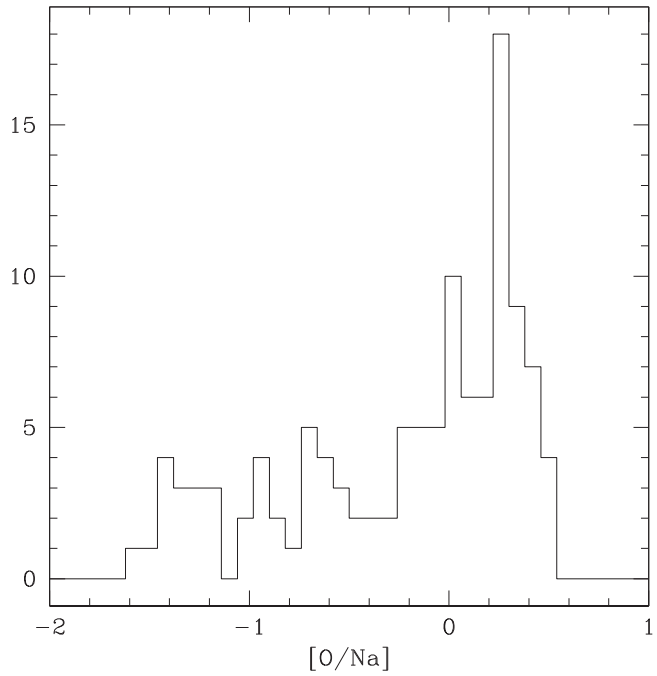

Figure 7. Distribution function of the [O/Na] ratios of 117 giants in NGC 2808.

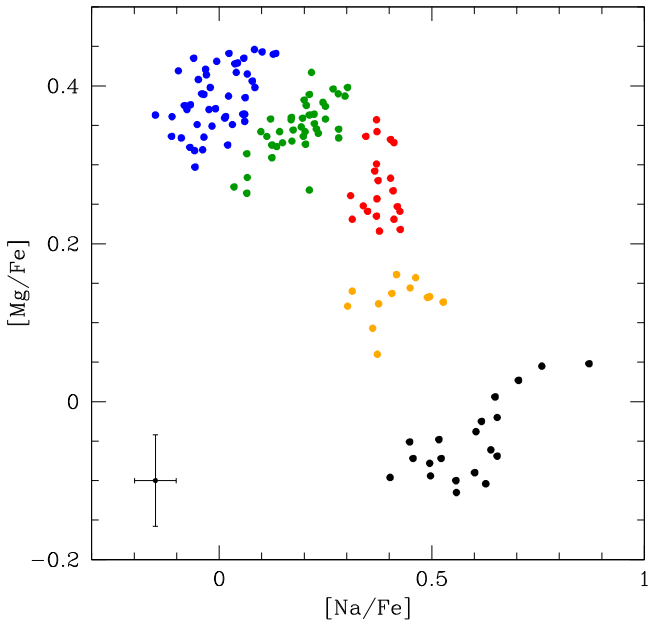

Figure 8. Anticorrelation between abundances of Mg and Na in RGB stars of NGC 2808. Different colors are used to indicate giants of different groups. Internal error bars are those derived for GIRAFFE, the ones relative to UVES being slightly smaller.

HB stars do not belong to the primordial cluster population, as expected from the classic paradigm relating O-rich stars to normal helium content. Recently, Marino et al. (2014), who did not derive O abundances for their sample of HB stars, confirmed a bimodality in Na among RHB stars in NGC 2808.

We may tentatively conclude that we found in our sample of RGB stars the progenitors of the two groups that end up on the RHB, with normal He, similarly high O, and slightly different Na content.

Two other groups seen in Figure 7 present a composition typical of intermediate second-generation stars, while the last is clearly identifiable with the extreme component as defined in Carretta et al. (2009c), characterized by very low O abundances and high Na values.

The coincidence of five groups distinct in their chemical compositions with five populations found photometrically by Milone et al. (2015) is a result beyond our expectations because this reanalysis was started simply to bring NGC 2808 onto the homogeneous system used for all other GCs in our FLAMES survey. Fortunately, we now have the possibility of investigating this finding in deeper detail using the abundances of other proton-capture elements as a sanity check, showing that there is not a simple correspondence between the results from spectroscopy and photometry. The scenario in NGC 2808 looks more complex.

3.2. The Na–Mg Anticorrelation Confirms Five Discrete Groups in NGC 2808

Several reasons prompted us to use the relation between Na and Mg abundances to check the reality of the five chemically distinct components on the RGB of NGC 2808. These elements are the outcome of two different cycles (NeNa and MgAl), so they sample different reactions occurring at different temperatures and thus mass stratifications. Their interplay is then a good candidate to offer a panoramic view over the whole mass range of possible polluters that contributed gas enriched in proton-capture elements at the epoch of cluster formation.

From a more practical point of view, all 140 giants in our final sample have Na abundances, and we cannot derive a Mg abundance only for one star, with a net gain of about 20% in statistics with respect to the O–Na plot.

The abundances of Na and Mg are plotted in Figure 8. The ratios [Na/Fe] and [Mg/Fe] in RGB stars of NGC 2808 are anticorrelated, with Mg decreasing by about 0.55 dex, while Na increases by about 1 dex. A Spearman correlation test provides a probability that Na and Mg are not anticorrelated of less than 1.0×10^{-6}. This feature is not surprising, apart from the large fraction of stars with severe Mg depletions in this GC, being simply the consequence of Na production from ^{22}Ne with simultaneous Mg consumption from the MgAl cycle. However, the key feature we observe in NGC 2808 is that the stars appear not to be uniformly distributed along the anticorrelation, but instead it looks like they are clustered in several distinct groups. In analogy with the division based on O and Na abundances, we call these five groups *P1*, *P2* (with primordial or almost primordial abundance ratios), *I1*, *I2* (with intermediate composition), and *E* (with severely extreme changes from the original composition).

To check this appearance, we examine the distribution function of the [Na/Mg] ratio in the left panel of Figure 9.

The distribution presents four clear peaks, with the group *I2* seen as a tail rightward of the *I1* groups, because these two groups have quite similar Na content, but with Mg abundances decreasing by about 0.2 dex from *I1* to *I2* (see Figure 8). A clearer representation of the five groups is given by the right panel of Figure 9, where we plot the distribution function relative to the quantity [Na/Fe]–2[Mg/Fe] to account for the fact that the spread in Na is almost twice the spread in Mg. This is a sort of pseudoratio, in analogy with pseudocolors used in photometry (see, e.g., Milone et al. 2015 and the references therein).

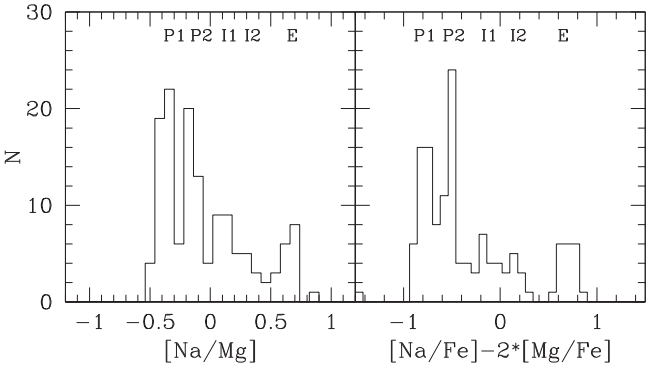

Figure 9. Left panel: distribution function of the [Na/Mg] ratio for RGB stars in NGC 2808. In the right panel is plotted the distribution of the quantity [Na/Fe]–2[Mg/Fe] for the same stars. The five peaks corresponding to the five groups along the Na–Mg anticorrelation are labeled.

In this case, all five groups are clearly separated, and this plot is a mirror image of Figure 7, assessing on a more robust statistical basis the presence of five groups of stars with distinct abundances of proton-capture elements on the RGB of NGC 2808.

We indicate with different colors in Figure 8 these components: blue (*P1*), green (*P2*), red (*I1*), orange (*I2*), and black (*E*).[2] The mean abundances for each group are listed in Table 7, where Al abundances available for 31 giants with UVES spectra are from Carretta (2014), with atmospheric parameters already on the present homogeneous scale.

The fraction of RGB stars in each group is $P1 = 33\% \pm 5\%$, $P2 = 29\% \pm 5\%$, $I1 = 15\% \pm 3\%$, $I2 = 9\% \pm 2\%$, and $E = 14\% \pm 3\%$. All groups are well defined and distinct in the Na–Mg plane. In Figure 10 we show how different they are by plotting the cumulative distributions of the [Na/Mg] ratio for the five components, using the same color coding as in Figure 8.

To put these differences on a quantitative foundation, we test with a Kolmogorov–Smirnov test the null hypothesis that any pair of the distributions is extracted from the same parent distribution in [Na/Mg]. This hypothesis is safely rejected in all cases, with the probabilities of rejecting it by mere chance given in the last column of Table 8.

4. DISCUSSION

The homogeneous reanalysis of 140 red giants allows us to uncover five different populations, with distinct chemical composition, on the RGB of NGC 2808, thanks to large statistics and a significant decrease in internal errors on abundances. We can look now in more detail at the properties of these components.

4.1. Chemical Tagging of the Five Groups on the RGB

The separation of RGB stars into five groups has been assessed from both the classic Na–O and the Na–Mg anticorrelations. The last was used to operatively define the five populations, and with this criterion we plotted with different color stars on the anticorrelations and the correlation among proton-capture elements Na, O, Mg, and Si in Figure 11.

The classification with the [Na/Mg] results in an efficient ranking of the five populations in all of the other abundance planes, ordering the *P1*, *P2*, *I1*, *I2*, and *E* groups with decreasing Mg and O abundances and increasing Na and Si abundances. The boundaries of the populations are, however, more neatly defined in the Na–Mg plane. Some "blurring" is present at the border between the primordial populations *P1* and *P2* when O is involved, although the bulk of the stars are well separated. The smearing of stars in *P1* and *P2* appears to be more severe with the Si abundances (bottom-right panel in Figure 11). However, this is expected because the production of ^{28}Si is not a main process in the proton-capture reactions, but only a leakage from the Mg–Al cycle (Karakas & Lattanzio 2003). When the bulk of abundances are still primordial, with the large overabundances of α elements from SNe II nucleosynthesis still in place, a slight enhancement in Si from ^{27}Al$(p,\gamma)^{28}$Si is not clearly discernible. However, as more severe changes in composition from the action of hot H burning start to appear among stars, the modification to the Si level also becomes more evident, as shown by stars of the *I1*, *I2*, and *E* populations.

The abundances of Mg and Al for the 31 giants with UVES spectra were derived in Carretta (2014) using the present homogeneous scale. The Mg–Al anticorrelation shows three clumps of stars with distinct chemical composition, and the three discrete populations account for $68\% \pm 15\%$, $19\% \pm 8\%$, and $13\% \pm 4\%$ of stars, for the *P*, *I*, and *E* components, respectively. A comparison with Carretta (2014) shows that the P stars along the Mg–Al anticorrelation are split among the present *P1* and *P2* groups, and the I stars among *I1* and *I2*, and finally the *E* stars in Carretta (2014) are found here to all belong to the *E* population (see Table 7) with severe Mg depletions. The fractions derived independently along the Mg–Al anticorrelation are in excellent agreement (within the associated Poisson errors) with the number counts for the total *P1*+*P2* (62%), *I1*+*I2* (24%), and *E* (14%) populations as defined here from the Na–Mg anticorrelation.

A more quantitative description of the chemical composition in the five populations of RGB stars is summarized in Table 8. We used Student's and Welch's tests to determine if two sets of data are significantly different from each other, for every one of the 10 combinations of the five groups. We tested the null hypothesis that any pair of components is extracted from a distribution having the same mean [element/Fe] for [Fe/H], [O/Fe], [Na/Fe], [Mg/Fe], [Al/Fe], [Si/Fe], and [Na/Mg]. For any combination and element we list the *t* value, the number of degrees of freedom, and the two-tailed probability.

The first consideration is that the metallicity [Fe/H] is the same for almost all populations. Only the value of the *E* population seems to be statistically different from the metallicity of the primordial and intermediate components. This result is in qualitative agreement with the findings of Bragaglia et al. (2010) in a large set of GCs and in NGC 2808 in particular, with the expectation that the extreme population *E* must be enhanced in helium. By consequence for a fixed global metallicity, a decrease in the H abundance is predicted, so the ratio [Fe/H] is expected to slightly increase.

[2] Star 46580, with [Na/Fe] = +0.212 dex and [Mg/Fe] = +0.268, may have a somewhat more uncertain definition because it is located in an intermediate position between the *P2* and *I1* groups. Looking at the ratios of the other elements, we assigned this star to the *P2* component. Star 55822, with no Mg determination, has [O/Fe] = −0.644 dex and [Na/Fe] = +0.608 dex, and it is very likely that this object belongs to the *E* component. Conservatively, we did not assign this star to any of the five groups. None of our results is, however, affected by these two objects.

Table 7
Average Abundances of Proton-capture Elements in the Five Groups on the RGB of NGC 2808

El.	*P1*	*P2*	*I1*	*I2*	*E*
	n avg. rms	*n* avg. rms	*n* avg. rms	*n* avg. rms	*n* avg. rms
[Fe/H]	46 −1.128 0.028	40 −1.134 0.026	21 −1.130 0.024	12 −1.137 0.028	20 −1.115 0.019
[O/Fe]	42 +0.308 0.058	35 +0.154 0.090	15 −0.216 0.124	7 −0.447 0.217	17 −0.656 0.161
[Na/Fe]	46 −0.005 0.067	40 +0.188 0.068	21 +0.378 0.034	12 +0.414 0.072	20 +0.592 0.112
[Mg/Fe]	46 +0.384 0.041	40 +0.346 0.035	21 +0.274 0.044	12 +0.127 0.028	20 −0.050 0.050
[Al/Fe]	12 +0.065 0.062	9 +0.273 0.132	4 +1.006 0.118	2 +1.079 0.108	4 +1.218 0.089
[Si/Fe]	46 +0.265 0.026	40 +0.262 0.026	21 +0.309 0.026	12 +0.346 0.038	20 +0.390 0.036
[Na/Mg]	46 −0.388 0.059	40 −0.158 0.051	21 +0.104 0.057	12 +0.287 0.069	20 +0.642 0.083

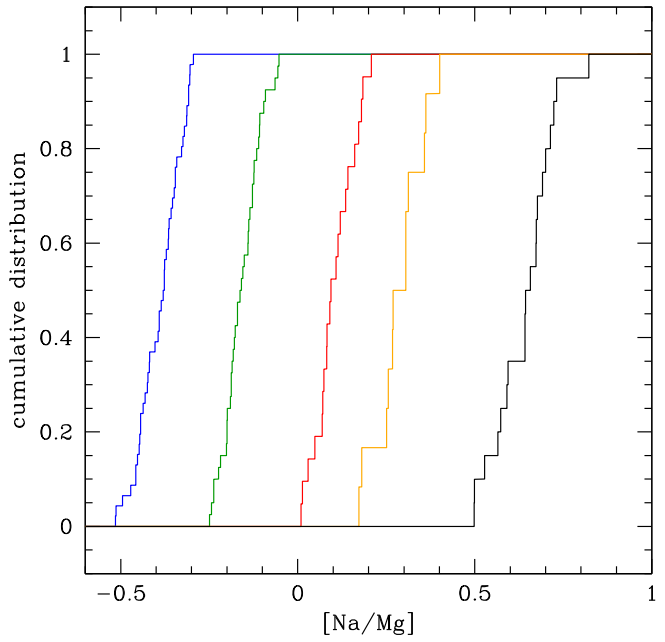

Figure 10. Cumulative distribution of the [Na/Mg] ratio in the five groups of RGB stars using the same color coding as in Figure 8: blue, green, red, orange, and black indicate groups *P1*, *P2*, *I1*, *I2*, and *E*, respectively.

Mean O abundances differ among all groups, and despite a couple of mutual interlopers (Figure 11, top left panel), the average abundances of populations *P1* and *P2* are statistically different. For Na, average abundances do not significantly differ only among the two intermediate populations *I1* and *I2*. The reality of this feature is also confirmed by the fact that their mean abundances of Al (that correlate with Na) are also not significantly different. As already noted by visual inspection of Figure 11, the mean [Si/Fe] ratio is similar for the primordial groups *P1* and *P2*, but it differs in any other case. Finally, the [Mg/Fe] and [Na/Mg] ratios are found to be statistically different in all populations at a very high level of confidence.

Each of the five populations selected from the Na–Mg plane seems to be a *single* stellar population. Following the approach used by Gratton et al. (2011) for RHB stars, typical (anti) correlations would be observable if a single group were composed of more than one population with homogeneous composition. We verified this issue by looking at the presence of a Mg–Na anticorrelation or a Mg–O correlation within each group. In each case we found either the reverse relation (Mg correlated with Na or anticorrelated with O) or the correct relation was found not to be statistically robust. Moreover, in each population the [Na/Mg] ratio presents a single peaked distribution.

Recently, Mucciarelli et al. (2015) (Mu15) derived potassium abundances for 116 giants of our sample in NGC 2808 (excluding three stars flagged as possible binaries). They found that this GC is the second one after NGC 2419 (Cohen & Kirby 2012; Mucciarelli et al. 2012) where a Mg–K anticorrelation is clearly observed. In Figure 12 we show our [Mg/Fe] ratios as a function of their [K/Fe] values, putting the Mg–K anticorrelation on a larger statistical basis and confirming that K in a few GCs participates in the same self-enrichment network due to proton-capture reactions. A more precise comparison with the results of Mucciarelli et al. (2015) is hampered by the fact that for NGC 2808 they used the older temperature scale by Carretta et al. (2006, 2009b). However, there is a way to bypass this obstacle.

The Si–Al correlation and the mirroring Mg–Si anticorrelation, observed in NGC 2808 and other GCs (Yong et al. 2005; Carretta et al. 2009b), are thermometers indicating that the temperature of the H burning generating this pattern exceeded $T_6 \sim 65$ K (Arnould et al. 1999), because at this temperature the reaction ^{27}Al(p,γ)^{28}Si becomes dominant over ^{27}Al(p,α)^{24}Mg. However, this is only a lower limit to the temperature, meaning that from now on the leakage of ^{28}Si from the Mg–Al cycle is possible. A more elevated temperature regime is required to explain the changes in the K content as observed in NGC 2419 (Ventura et al. 2012). In their attempt to account for the extreme K-enhanced, Mg-depleted stars observed by Mucciarelli et al. (2012), Ventura et al. postulated that at temperatures above 10^8K is activated a process of proton capture on ^{36}Ar that produces potassium and shifts the equilibrium among various species toward heavier nuclei like K, Ca, and Sc, in particular when low-metallicity models are considered. The effect is relevant on K (see Figure 12) and on Sc because they are much less abundant than Ca: a fraction of the original Ar is sufficient to provide a large abundance variation. The case of Ca is different because the original content of this element is larger than that of K and much more abundant than Sc.

Hence, if this process were at work also in (at least some) first-generation stars at the higher metallicity of NGC 2808, we could test it by using our homogeneous set of abundances without being afraid of possible offsets between different analyses, as for K, since with the same scale we derived in the present work the abundances of Sc, Mg, Si, and Ca. The relations between these elements are shown in Figure 13. The probability that Sc and Mg are not anticorrelated is $P = 1.0 \times 10^{-8}$, whereas that of Sc and Si lacking a correlation is $P = 0.0$. For the correlation Sc–Ca we found $P = 3.5 \times 10^{-5}$, with 140 dof. Finally, the correlations of Sc and Si with K are both found to be statistically significant. We may conclude that clear evidence does exist for the action of

Table 8
t values, Degrees of Freedom, and Two-tailed Probability Values for the Student *t*-test on the Mean Abundance Ratios for the Five Groups in NGC 2808

Groups	[Fe/H]	[O/Fe]	[Na/Fe]	[Mg/Fe]	[Al/Fe]	[Si/Fe]	[Na/Mg]	Prob(K–S)
P1–P2	1.03	8.73	13.22	4.64	4.38	0.53	19.39	3.5×10^{-20}
d.f.	84	75	84	84	19	84	84	
p	0.306	0.00	0.00	1.2×10^{-5}	3.2×10^{-4}	0.598	0.00	
P1–I1	0.30	15.76	31.00	9.69	15.26	6.43	32.41	6.0×10^{-14}
d.f.	65	55	65	65	14	65	65	
p	0.765	0.00	0.00	0.00	0.00	2.0×10^{-8}	0.00	
P1–I2	0.99	9.15	18.21	25.46	12.93	6.97	31.06	1.5×10^{-9}
d.f.	56	47	56	56	12	56	56	
p	0.326	0.00	0.00	0.00	2.0×10^{-8}	1.5×10^{-5}	0.00	
P1–E	2.19	24.06	22.18	34.15	24.04	14.02	50.25	1.6×10^{-13}
d.f.	64	57	64	64	14	64	64	
p	0.032	0.00	0.00	0.00	0.00	0.00	0.00	
P2–I1	0.60	10.44	14.54	6.50	9.96	6.71	17.67	32.3×10^{-13}
d.f.	59	48	59	59	11	59	59	
p	0.551	0.00	0.00	2.0×10^{-8}	7.7×10^{-7}	0.00	0.00	
P2–I2	0.33	7.20	9.66	22.36	9.14	7.17	20.71	2.7×10^{-9}
d.f.	50	40	50	50	9	50	50	
p	0.743	1.0×10^{-8}	0.00	0.00	7.5×10^{-6}	0.00	0.00	
P2–E	3.21	19.33	14.82	31.74	15.10	14.16	39.53	5.6×10^{-13}
d.f.	58	50	58	58	11	58	58	
p	0.002	0.00	0.00	0.00	1.0×10^{-8}	0.00	0.00	
I1–I2	0.73	2.62	1.63	11.71	0.76	3.00	7.79	7.0×10^{-6}
d.f.	31	20	31	31	4	31	31	
p	0.471	0.016	0.113	0.00	0.490	0.005	1.0×10^{-8}	
I1–E	2.22	8.71	8.19	21.98	2.87	8.22	24.08	3.3×10^{-10}
d.f.	39	30	39	39	6	39	39	
p	0.032	0.00	0.00	0.00	0.028	0.00	0.00	
I2–E	2.41	2.30	7.96	12.83	1.57	3.23	13.04	1.0×10^{-7}
d.f.	30	22	30	30	4	30	30	
p	0.022	0.031	1.0×10^{-8}	0.00	0.192	0.003	0.00	

Note. In the last column the probabilities of a K–S test on cumulative distributions of [Na/Mg] are also listed.

proton capture occurring at a particularly high temperature regime in the portion of stars that contributed to the pollution of intracluster gas at the epoch of the formation of the following generation(s) of stars. A clue on the origin of this processed material is, however, hard to assess since such temperatures are encountered in the two main candidate polluters proposed for GCs, namely massive AGBs and the most massive main-sequence stars (see Prantzos et al. 2007).

The cases of NGC 2419 and NGC 2808 point out, albeit to a different degree, the key role of Mg depletion as a useful indicator of a particular environment where the network of proton-capture reactions operates at unusually high temperature. We may then confirm the plot in Figure 14, first introduced in Carretta et al. (2013b), as a powerful diagnostic to uncover GCs where this extreme processing occurred. In this plot we compare one of the elements most affected by this advanced nucleosynthesis, Mg, with one of the least varied, Ca. Using as a reference the homogeneous analysis of more than 280 RGB stars with UVES spectra in 23 GCs (green squares), it is possible to pick up clusters where signatures of such a particular nucleosynthesis are visible. Apart from the exceptional case of NGC 2419, only NGC 2808, NGC 4833, and M15 stand out, with the last two GCs being much more metal-poor.

4.2. Comparison with Photometry

Milone et al. (2015) identified at least five clumps of stars on the RGB in NGC 2808 from precise UV photometry with *HST* and color or pseudocolor indexes purposely tailored to maximize the separation among photometric sequences due to the absorption of molecular bands like OH, NH, CN, and CH of elements involved in proton-capture reactions. The counterparts of these discrete populations are also found among MS stars, although less clearly since molecular bands become less prominent in warmer stars. Using 32 giants in their set with abundances from Carretta et al. (2004, 2006) and Carretta (2014), Milone et al. showed that their populations from *B* to *E* present signatures of increasingly processed composition, namely depletions in O and Mg and enhancements in Na and Al. The metallicity and composition of their population *A* is unknown, lacking stars with spectroscopy, but they inferred a primordial abundance pattern in this group.

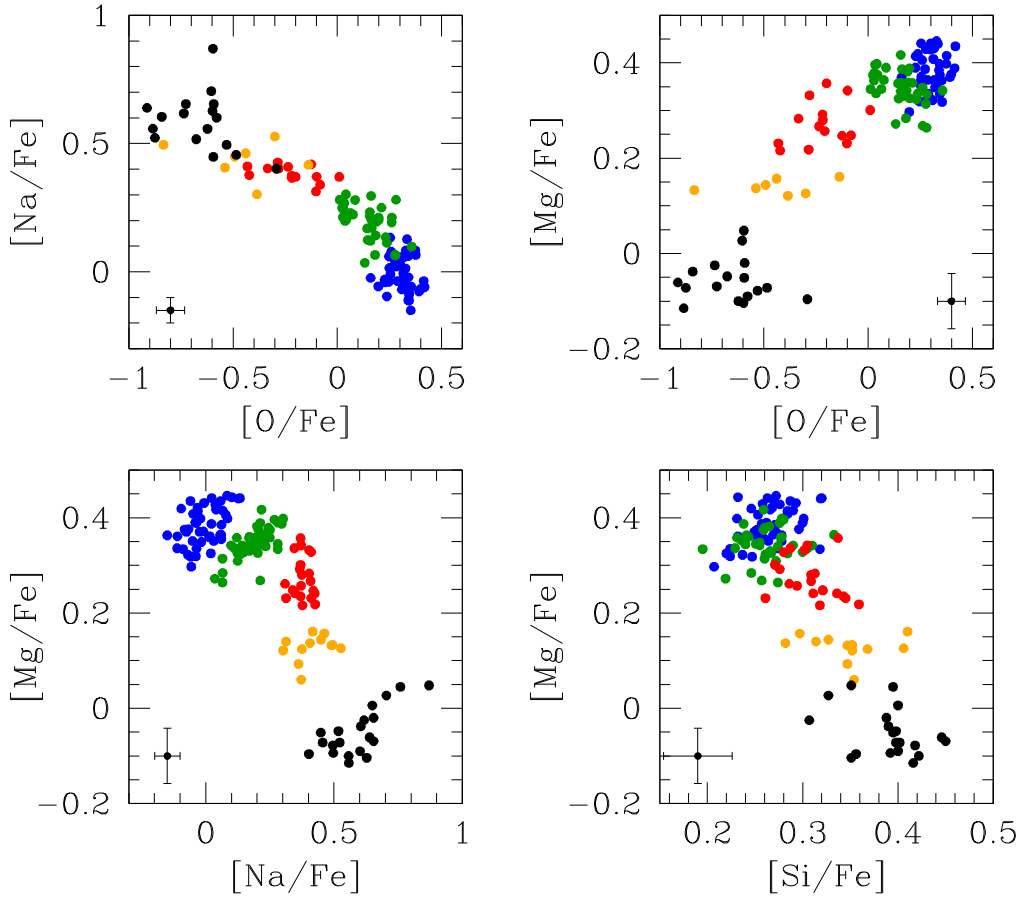

Figure 11. From bottom left and clockwise: Mg–Na and Na–O anticorrelations, Mg–O correlation, and Mg–Si anticorrelation among RGB stars in NGC 2808. Different colors indicate the five populations as defined in the Na–Mg plane. In each panel the star-to-star error bars are indicated.

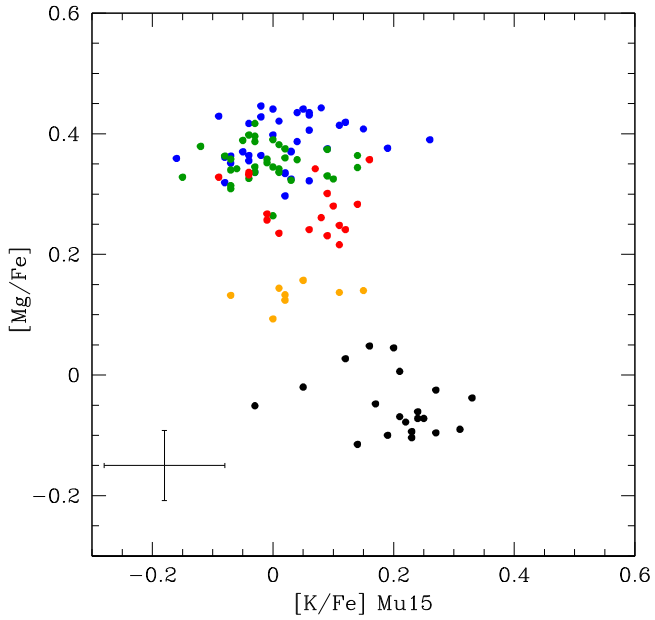

Figure 12. Ratio [Mg/Fe] as a function of the [K/Fe] ratio from Mucciarelli et al. (2015) in giants of NGC 2808, using the same color coding of Figure 8 for stars of populations *P1*, *P2*, *I1*, *I2*, and *E*.

A direct comparison is difficult because the photometric catalogs are not yet published and usually *HST* fields are taken on the cluster center, with scarce overlap with the pointings of

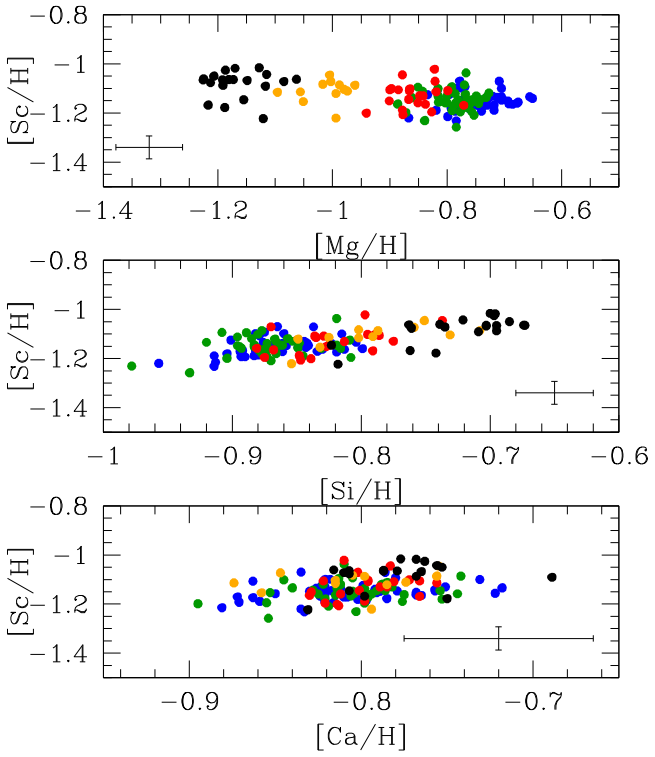

Figure 13. From top to bottom, Sc as a function of the abundances of Mg, Si, and Ca in our sample. Internal error bars are shown in each panel.

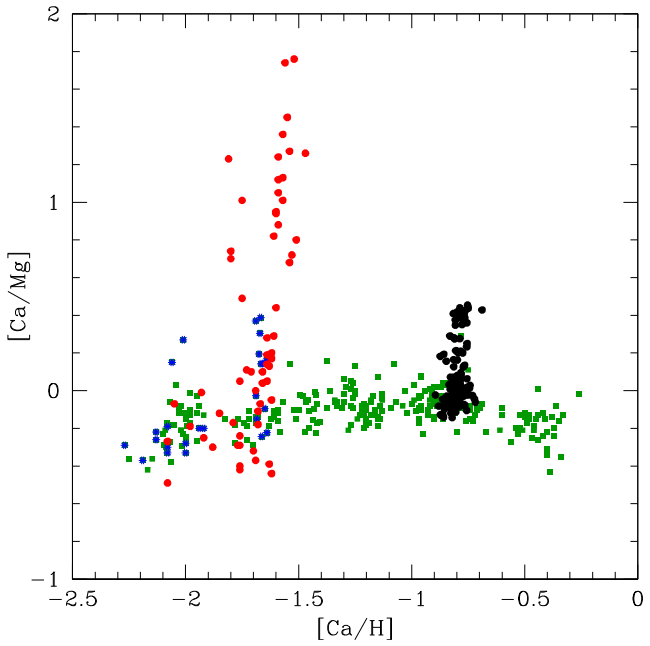

Figure 14. Ratio [Ca/Mg] as a function of the [Ca/H] ratio for giants in NGC 2419 (red filled circles; Cohen & Kirby 2012; Mucciarelli et al. 2012), in about 280 RGB stars in more than 20 GCs (Carretta et al. 2009b, 2010c, 2010a, 2011, 2013a, 2014, 2015; green squares), and giants in NGC 2808 (present work; black circles). Blue asterisks indicate M15 and NGC 4833.

multiobject spectrographs like FLAMES. However, we can use the 32 stars in common to bridge the gap and compare the five groups detected photometrically to the five populations with distinct composition uncovered in the present work. For each group of stars associated by Milone et al. (2015) to populations *B*, *C*, *D*, and *E,* we recomputed the average and rms scatter of the [O/Fe], [Na/Fe], [Mg/Fe], and [Si/Fe] ratios using the presently derived new abundances. Al was not considered because only a few stars from Carretta (2014) are in the photometric sample (all in the primordial regime, three in group *B* and two in *C*). We used these values simply to locate the position of the photometric groups in the upper half of the four panels in Figure 15, representing each group as a Gaussian centered at the elemental mean ratio and having the corresponding rms scatter as σ.

In the bottom half of each panel, we plotted the position of our five populations using the values in Table 7. This comparison shows that the match is satisfactory but not perfect. The cross-identification of a few populations, namely the extreme components, seems to be firmly established. The two groups *P1* and *P2* with primordial or almost primordial composition correspond to the populations *B* and *C*, respectively, for each of the four elements. We may conclude that the parent populations of the two groups of RHB stars in NGC 2808 are then traced on the RGB using both photometry and spectroscopy. Also, the extreme population is easily (and unambiguously) identified in the present work and in the *HST* photometry by Milone and collaborators.

Some problems seem to arise when dealing with the intermediate components. In the panels of Figure 15 for O, Mg, and Si, the photometric component *D* looks more or less coincident with our population *I2*, but in these plots it seems difficult to trace among the photometric groups the counterpart of *I1*, the other population with intermediate composition. On the other hand, when looking at Na, the photometric group *D* seems to be associated more with the *I1* population than with *I2*. However, this mismatch may actually be only apparent because in Figure 3 of Milone et al. (2015) group *D* shows a large spread in the index $\Delta_{\rm F336W,F438W}$, with a tail visible at low values. Since this index is sensitive to the abundances of light elements (C, N), it is also likely that group *D* is not a simple stellar population, as already stated for groups *B* and *C* by Milone et al.

In Table 9 we summarized recent results from spectroscopy and photometry to estimate the number of components detected in different evolutionary phases in NGC 2808 and the fractions of stars attributed to each one. Despite the variety of methods and evolutionary phases sampled, a few facts emerge.

First, NGC 2808 hosts the largest fraction of stars with primordial composition observed among massive Milky Way GCs to date: about 50% of the currently observed stellar population belongs to the original generation formed in this object. This feature is clearly appreciated in Figure 16, based on the now fully homogeneous analysis of Na and O abundances for 1598 red giants in 24 GCs from our FLAMES survey, where we plot the fraction of stars in the *P* component as a function of metallicity. The estimates for NGC 2808 range from about 41% from the number count on the RHB (Iannicola et al. 2009; Dalessandro et al. 2011) up to the maximum value of 68% derived from the Mg–Al anticorrelation in RGB stars (Carretta 2014). Even such a high value seems, however, confirmed by number counts on the red MS (Milone et al. 2012b). Since on average the stellar primordial content in GCs is much lower (about 30% as estimated from the Na–O anticorrelation), an open question is how and why NGC 2808 retained such a higher fraction.

The second feature inferred from Table 9 is that a gross division into three components seems to be accounted for by most analyses. For the intermediate group, with clearly modified but not extreme chemical composition, a fraction ranging from one-fifth up to one-third is observed by most studies. The extreme component is also traced (whenever accessible to observations) by most works, with reassuringly similar estimates of the fraction of stars.

However, a third fact is assessed by recent studies, although hints were already suggested by early investigations of the multimodal HB in NGC 2808: a finer subdivision of components is corroborated from high-precision photometry and spectroscopy. The cross match between abundances and color indexes is usually good and mutually suggests that what we are observing are real stellar populations forming discrete sequences or groups.

5. SUMMARY AND CONCLUSIONS

From high/intermediate spectra we reanalyzed 140 individual RGB stars in NGC 2808 using the same homogeneous procedures adopted for more than 2500 giants in the other 23 GCs. We derived abundances of Fe, O, Na, Mg, Si, Ca, Sc, Ti, Cr, Mn, and Ni. Pure α elements and elements of the Fe group are constant among multiple populations in NGC 2808. On our high-resolution UVES metallicity scale (Carretta et al. 2009a), we found a metal abundance for NGC 2808 of [Fe/H] $= -1.129$ ±0.005 ±0.034 ($\pm$ statistical $\pm$ systematic error) with $\sigma = 0.030$ (31 stars).

We confirm that the Na–O anticorrelation in this cluster is one of the most extended observed in GCs with no intrinsic spread in iron, in agreement with the high cluster present-day

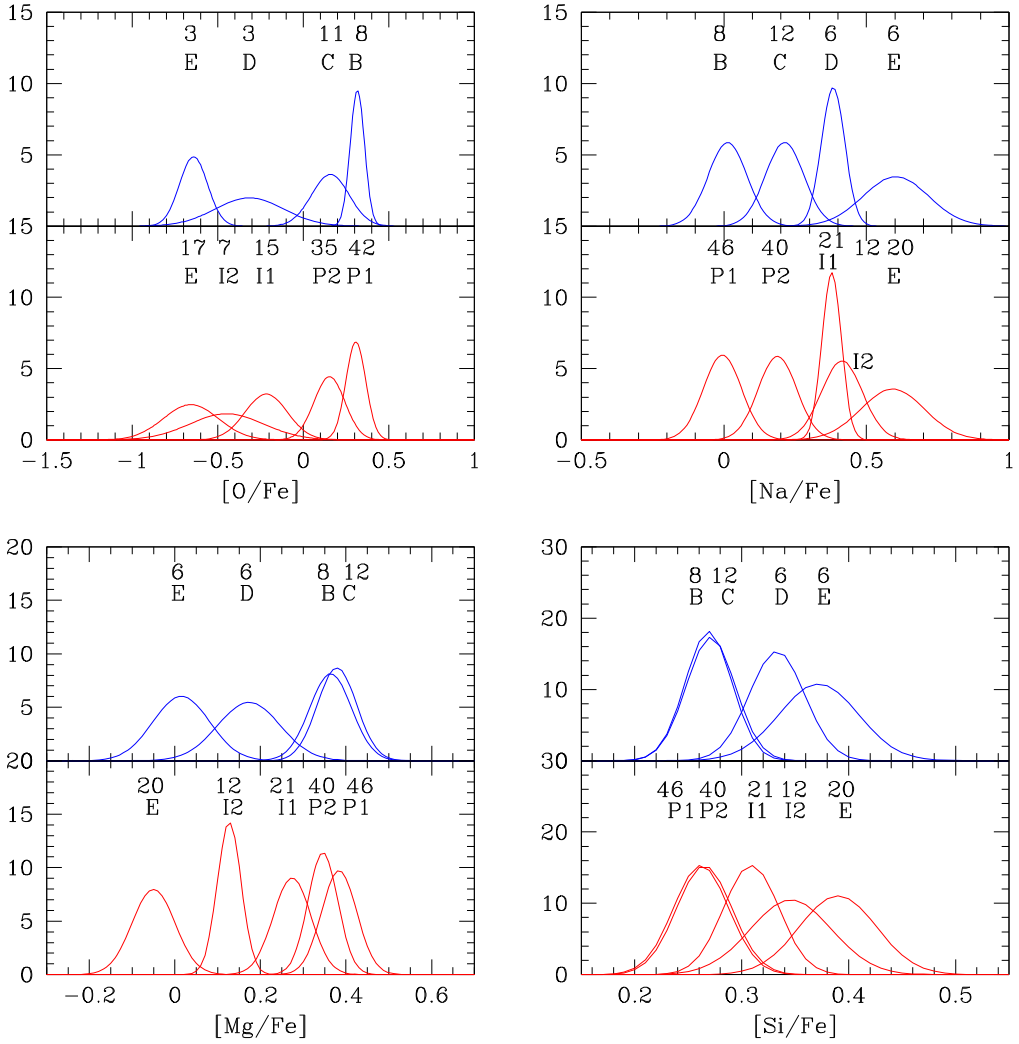

Figure 15. Comparison of mean abundance ratios for the photometric populations *B*, *C*, *D*, and *E* identified by Milone et al. (2015; upper half of each panel) with average ratios of the five populations *P1*, *P2*, *I1*, *I2*, and *E* (lower half of each panel). Each population is represented by a Gaussian centered at the mean value and with σ given by the rms scatter of the mean ratio.

total mass and with the hot temperatures reached on the blue HB. According to the definition of Carretta et al. (2009c), NGC 2808 hosts the highest fraction of primordial, first-generation stars detected spectroscopically. The improved statistics and the smaller internal errors due to uncertainties in the analysis uncover that the stars along the Na–O anticorrelation seem to be clustered in five groups.

The larger sample of stars with Na and Mg abundances allows us to confirm that five populations of RGB stars with distinct compositions of proton-capture elements are located along the Na–Mg anticorrelation. Statistical tests provide robust evidence of the different chemistry of these components, which we called *P1*, *P2*, *I1*, *I2*, and *E* in order of decreasing Mg and increasing Na abundances. Large Mg depletions are observed in NGC 2808, with a fraction of about 14% of stars (the *E* component) having solar or even subsolar [Mg/Fe] ratios.

We confirm and extend in statistics the anticorrelation between Mg and potassium abundances found by Mucciarelli et al. (2015) in this GC. Mg anticorrelated with K and Si, as well as with Sc, is proof that proton-capture processes operated in a very elevated temperature regime for H burning in some of the stars of the first generation in NGC 2808.

The match of the five populations detected from spectroscopy and the five groups recently discovered by Milone et al. (2015) with UV photometry is good but not perfect. The two populations with almost primordial abundances are well cross-identified, nicely tracing the progenitors of the two groups of RHB stars individuated by Gratton et al. (2011) and Marino et al. (2014). There is also a definite agreement on the extreme component. The partial mismatch of the populations with intermediate composition confirm the evidence that other discrete components may exist in NGC 2808, as suggested by the photometry.

Apparently, current modeling seems to lag somewhat behind observations. The strong depletions detected in NGC 2808 (Carretta 2014, and the present analysis) offer a severe challenge to the main scenario of self-enrichment of GCs in early epochs. Models of asymptotic giant branch (AGB) or SAGB stars with the proper metallicity ($Z = 0.001$) produce the required depletions in Mg (Ventura et al. 2013), but not enough to match the reduction factors observed in NGC 2808. On the other hand, the wind from model 60rD in the set of fast-rotating

Table 9
Stellar Populations in NGC 2808

		Spectroscopy		
Na–O RGB	*P*	*I*	*E*	
Fraction	45% ± 6%	36% ± 6%	18% ± 4%	this work
Na–Mg RGB	*P1 P2*	*I1 I2*	*E*	
Fraction	33% ± 5% 29% ± 5%	15% ± 3% 9% ± 2%	14% ± 3%	this work
Mg–Al RGB	*P*	*I*	*E*	
Fraction	68% ± 15%	19% ± 8%	13% ± 4%	Carretta 2014
from O RGB	O-normal	O-poor	super O-poor	
Fraction	61% ± 17%	22% ± 4%	17% ± 4%	Carretta+ 2006
Na–O HB	RHB O-rich/Na-poor moderate Na–O anticorrelation	BHB O-poor/Na-rich		Gratton+ 2011
Na–O HB	RHB lower Na bimodal Na	BHB higher Na higher He		Marino+ 2014
K in RGB	Primordial low K	Intermediate intermediate K	Extreme high K	Mucciarelli+ 2015
		Photometry		
MS	rMS	mMS	bMS	
Fraction	62% ± 2%	24% ± 2%	14% ± 3%	Milone+ 2012
AGB	AGB(I)	AGB(II)	AGB(III)	
Fraction	49% ± 11%	22% ± 6%	29% ± 8%	Milone+ 2015
AGB	*A B C*	*D*	*E*	
Fraction	*A*5.8% ± 0.5% *B*17.4% ± 0.9% *C*26.4% ± 1.2%	31.3% ± 1.3%	19.1% ± 1.0%	Milone+ 2015
Estimate	*A B C*	*D*	*E*	
From MS	$Y = 0.246$ 0.278 0.280	$Y = 0.329$	$Y = 0.384$	Milone+2015
From RGB	$Y = 0.243$ 0.278 0.280	$Y = 0.318$	$Y = 0.367$	
From HB	RHB	BHB	EHB	
Fraction	41% ± 3%	39% ± 3%	9% ± 1%	Dalessandro+ 2011
Estimate	$Y = 0.248$	$Y = 0.30$	$Y = 0.40$	
From HB	RHB	EBT1	EBT2	
Fraction	41% ± 3%	34% ± 2%	14% ± 1%	Iannicola+ 2009
From HB	RHB	EBT1	EBT2	
Fraction	50%	30%	20%	D'Antona+ 2005
Estimate	$Y = 0.24$	$Y = 0.26$–0.29	$Y = 0.40$	
From HB	RHB	EBT1	EBT2	
Fraction	46% ± 10%	35% ± 10%	10% ± 5%	Bedin+ 2000

Note. Residual components on the HB are as follows: EBT3 9% ± 5% (Bedin+2000); BHk 9% ± 1% (blue hook stars, Dalessandro+2011); EBT3 11% ± 1% (Iannicola+2009).

massive stars by Decressin et al. (2007) seems to be able to account for a large range of Mg depletions and Al enhancement, but at the price of a strong destruction of Na, which is not observed in stars of NGC 2808 with extreme composition (this work and Carretta 2014). For the time being, we note that Bastian et al. (2015) showed how not one of the most fashionable models proposed for polluting first-generation stars is able to fit at the same time the abundance pattern of normal GCs and the extreme modifications observed in NGC 2808. Once again, this cluster is a pivotal object in interpreting the evidence of multiple populations in GCs.

The discreteness of the different populations detected in NGC 2808 (see Table 9) presents another level of challenge. In most scenarios (see Gratton et al. 2012), the observed

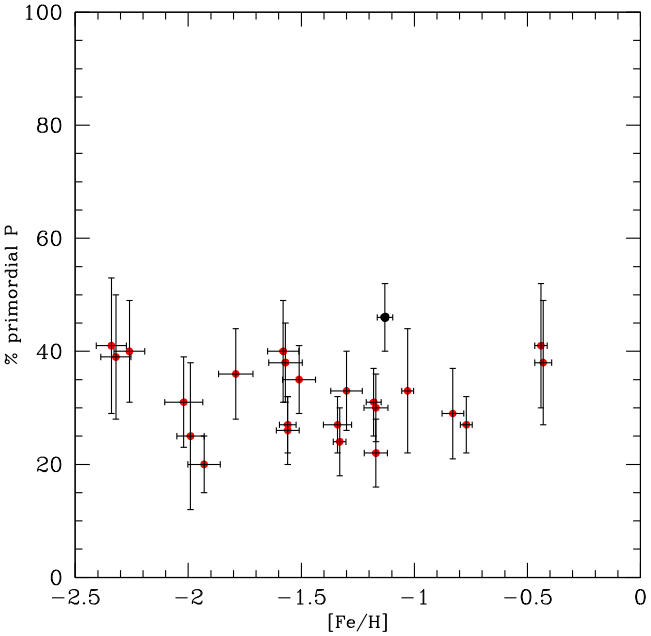

Figure 16. Fractions of first-generation stars in 24 GCs of our FLAMES survey as a function of the metallicity [Fe/H]. The attached error bars in fractions are from Poisson statistics. For metallicity we used systematic errors (from Table 3 and similar tables in the other papers). NGC 2808 is indicated with a larger black symbol.

abundance pattern only may be approximated by diluting ejecta of favorite candidate polluters with unprocessed, primordial matter. It seems difficult to explain populations with discrete compositions by imagining a formation history where bursts of star formation are followed by multiple quiescent periods, whereas at the same time the abundances continue to change from one population to the next, following an empirical dilution model. To the difficulty of accounting for the origin and collection of pristine gas (e.g., D'Ercole et al. 2011), one is forced to add mechanisms to selectively stop the mixing and/or star formation several times in a few 10^7–10^8 years at the cluster formation.

A more definitive answer to the questions aroused by these recent discoveries in NGC 2808 must necessarily await the publication of photometric catalogs and the analysis of spectroscopic observations of stars in the photometric groups completed by Milone, Marino, and coworkers. Our group just gathered high-resolution, high-S/N spectra for about 100 giants in the present sample to measure Al abundances, already proved in NGC 6752 (Carretta et al. 2012) and NGC 2808 (Carretta 2014) to be very useful to chemical tagging of discrete stellar populations on the RGB. With the full set of elements involved in proton-capture reactions, we will be able to perform a statistically sound cluster analysis and hopefully disclose other windows on this very particular GC.

We thank Angela Bragaglia for valuable help and discussions and Alessio Mucciarelli for providing his results for potassium. This publication makes use of data products from the 2MASS, which is a joint project of the University of Massachusetts and the Infrared Processing and Analysis Center/California Institute of Technology, funded by the National Aeronautics and Space Administration and the National Science Foundation. This research has been funded by PRIN MIUR 2010-2011, project "The Chemical and Dynamical Evolution of the Milky Way and Local Group Galaxies" (PI F. Matteucci) . This research has made use of the SIMBAD database, operated at CDS, Strasbourg, France and of NASA's Astrophysical Data System.

REFERENCES

Alonso, A., Arribas, S., & Martinez-Roger, C. 1999, A&AS, 140, 261
Alonso, A., Arribas, S., & Martinez-Roger, C. 2001, A&A, 376, 1039
Arnould, M., Goriely, S., & Jorissen, A. 1999, A&A, 347, 572
Bastian, N., Cabrera-Ziri, I., & Salaris, M. 2015, MNRAS, 449, 3333
Bedin, L. R., Piotto, G., Zoccali, M., et al. 2000, A&A, 363, 159
Bragaglia, A., Carretta, E., Gratton, R. G., et al. 2001, AJ, 121, 327
Bragaglia, A., Carretta, E., Gratton, R. G., et al. 2010, A&A, 519, 60
Carretta, E. 2006, AJ, 131, 1766
Carretta, E. 2014, ApJL, 795, L28
Carretta, E., Bragaglia, A., & Cacciari, C. 2004, ApJL, 610, L25
Carretta, E., Bragaglia, A., Cacciari, C., & Rossetti, E. 2003, A&A, 410, 143
Carretta, E., Bragaglia, A., Gratton, R., et al. 2010a, ApJL, 712, L21
Carretta, E., Bragaglia, A., Gratton, R. G., D'Orazi, V., & Lucatello, S. 2009a, A&A, 508, 695
Carretta, E., Bragaglia, A., Gratton, R. G., & Lucatello, S. 2009b, A&A, 505, 139
Carretta, E., Bragaglia, A., Gratton, R. G., Lucatello, S., & D'Orazi, V. 2012, ApJL, 750, L14
Carretta, E., Bragaglia, A., Gratton, R. G., Lucatello, S., & Momany, Y. 2007a, A&A, 464, 927
Carretta, E., Bragaglia, A., Gratton, R. G., et al. 2006, A&A, 450, 523
Carretta, E., Bragaglia, A., Gratton, R. G., et al. 2007b, A&A, 464, 939
Carretta, E., Bragaglia, A., Gratton, R. G., et al. 2007c, A&A, 464, 967
Carretta, E., Bragaglia, A., Gratton, R. G., et al. 2009c, A&A, 505, 117
Carretta, E., Bragaglia, A., Gratton, R. G., et al. 2010b, A&A, 516, 55
Carretta, E., Bragaglia, A., Gratton, R. G., et al. 2010c, A&A, 520, 95
Carretta, E., Bragaglia, A., Gratton, R. G., et al. 2013a, A&A, 557, A138
Carretta, E., Bragaglia, A., Gratton, R. G., et al. 2014, A&A, 564, A60
Carretta, E., Bragaglia, A., Gratton, R. G., et al. 2015, A&A, 578, A116
Carretta, E., Gratton, R. G., Bragaglia, A., et al. 2013b, ApJ, 769, 40
Carretta, E., Lucatello, S., Gratton, R. G., Bragaglia, A., & D'Orazi, V. 2011, A&A, 533, 69
Carretta, E., Recio-Blanco, A., Gratton, R. G., Piotto, G., & Bragaglia, A. 2007d, ApJL, 671, L125
Cohen, J. G., & Kirby, E. N. 2012, ApJ, 760, 86
Dalessandro, E., Salaris, M., Ferraro, F. R., et al. 2011, MNRAS, 410, 694
D'Antona, F., Bellazzini, M., Caloi, V., et al. 2005, ApJ, 631, 868
Decressin, T., Meynet, G., Charbonnel, C., Prantzos, N., & Ekstrom, S. 2007, A&A, 464, 1029
Denisenkov, P. A., & Denisenkova, S. N. 1989, A. Tsir, 1538, 11
D'Ercole, A., D'Antona, F., & Vesperini, E. 2011, MNRAS, 415, 1304
Gratton, R. G. 1988, Rome Obs. Preprint Ser., 29
Gratton, R. G., Bonifacio, P., Bragaglia, A., et al. 2001, A&A, 369, 87
Gratton, R. G., Carretta, E., & Bragaglia, A. 2012, A&ARv, 20, 50
Gratton, R. G., Carretta, E., Claudi, R., Lucatello, S., & Barbieri, M. 2003, A&A, 404, 187
Gratton, R. G., Carretta, E., Eriksson, K., & Gustafsson, B. 1999, A&A, 350, 955
Gratton, R. G., Lucatello, S., Bragaglia, A., et al. 2006, A&A, 455, 271
Gratton, R. G., Lucatello, S., Bragaglia, A., et al. 2007, A&A, 464, 953
Gratton, R. G., Lucatello, S., Carretta, E., et al. 2011, A&A, 534, 123
Gratton, R. G., Sneden, C., Carretta, E., & Bragaglia, A. 2000, A&A, 354, 169
Grundahl, F., VandenBerg, D. A., & Andersen, M. I. 1998, ApJL, 500, L179
Han, S.-I., Lee, Y.-W., Joo, S.-J., et al. 2009, ApJL, 707, L190
Harris, W. E. 1996, AJ, 112, 1487
Iannicola, G., Monelli, M., Bono, G., et al. 2009, ApJL, 696, L120
Karakas, A. I., & Lattanzio, J. C. 2003, PASA, 20, 279
Kraft, R. P. 1994, PASP, 106, 553
Kurucz, R. L. 1993, CD-ROM 13, Smithsonian Astrophysical Observatory, Cambridge
Langer, G. E., Hoffman, R., & Sneden, C. 1993, PASP, 105, 301
Lee, J.-W., Lee, J., Kang, Y.-W., et al. 2009, ApJL, 695, L78
Magain, P. 1984, A&A, 134, 189
Marino, A. F., Milone, A. P., Przybilla, N., et al. 2014, MNRAS, 437, 1609
Marino, A. F., Villanova, S., Piotto, G., et al. 2008, A&A, 490, 625
Milone, A., Piotto, G., Bedin, L., et al. 2012a, ApJ, 744, 58
Milone, A., Piotto, G., Bedin, L., et al. 2012b, A&A, 537, A77
Milone, A. P., Marino, A. F., Piotto, G., et al. 2015, ApJ, 808, 51

Monelli, M., Milone, A. P., Stetson, P. B., et al. 2013, MNRAS, 431, 2126
Mucciarelli, A., Bellazzini, M., Ibata, R., et al. 2012, MNRAS, 426, 2889
Mucciarelli, A., Bellazzini, M., Merle, T., et al. 2015, ApJ, 801, 68
Nataf, D., Gould, A. P., Pinsonneault, M. H., & Udalski, A. 2011, ApJ, 766, 77
Pasquini, L., Avila, G., Blecha, A., et al. 2002, Msngr, 110, 1
Piotto, G., Bedin, L., Anderson, J., et al. 2007, ApJL, 661, L53
Piotto, G., Milone, A. P., Bedin, L. R., et al. 2015, AJ, 149, 91
Prantzos, N., Charbonnel, C., & Iliadis, C. 2007, A&A, 179, 190
Recio-Blanco, A., Aparicio, A., Piotto, G., De Angeli, F., & Djorgovski, S. G. 2006, A&A, 452, 875
Skrutskie, M. F., Cutri, R. M., Stiening, R., et al. 2006, AJ, 131, 1163
Smith, G. H. 1987, PASP, 99, 67
Sneden, C. 2000, in Proc. 35th Liege Int. Astrophysics Coll. 1999, The Galactic Halo: From Globular Cluster to Field Stars, ed. A. Noels et al. (Belgium: Liege), 159
Tukey, J. W. 1977, Explanatory Data Analysis (Reading, MA: Addison-Wesley)
Ventura, P., D'Antona, F., Di Criscienzo, M., et al. 2012, ApJL, 761, L30
Ventura, P., Di Criscienzo, M., Carini, R., & D'Antona, F. 2013, MNRAS, 431, 3642
Yong, D., Grundahl, F., Nissen, P. E., Jensen, H. R., & Lambert, D. L. 2005, A&A, 438, 875